

THE DETERMINATION OF MONOLAYER STRUCTURE BY INFRARED SPECTROSCOPY: CO₂ ON NaCl(100)

Otto BERG and George E. EWING *

Chemistry Department, Indiana University, Bloomington, IN 47405, USA

Received 13 March 1989; accepted for publication 1 May 1989

Infrared spectra of a ¹²C¹⁶O₂ monolayer on NaCl(100) are reported for the first time. The polarization and coverage dependence of spectroscopic signals indicate that there is only one kind of adsorption site, in which the molecular axis is tilted 68° from the surface normal. The adsorbate layer grows in the form of constant-density islands. Plane group symmetry analysis reveals a unique structure: there are two tilted molecules per layer unit cell, arranged in herringbone fashion. This structure is in quantitative agreement with the photometric observations. Splitting of the molecular ν₃ band is interpreted by a vibration–vibration coupling mechanism.

1. Introduction

Infrared spectroscopy is an effective probe of molecules physisorbed on alkali halide crystals. Vibrational spectra contain information regarding adsorbate geometry, surface bonding, and energy transfer processes. Most data of this kind have been obtained from substrates in the form of polycrystalline, porous films [1–5]. The principal advantage of these films is their large surface area and the resulting high optical density of adsorbates. The principal disadvantage is their uncertain or heterogeneous surface structure.

Recently, infrared spectra have been obtained using macroscopic single crystals as substrates [6,7]. Our group has studied the adsorption of carbon monoxide on NaCl(100) in detail [8,9]. The single-crystal experiment has three outstanding characteristics. First, the exposed (100) face is clean and large. Its adsorption sites form an extended regular array, and the fraction of defective sites is very small. Second, the crystal is macroscopically orientable. Adsorption geometry can now be probed directly by the polarization dependence of spectroscopic signals. Finally, photometric measurements of physisorbed CO show that the infrared oscillator strength is close to that of the gas phase molecule.

* To whom correspondence may be addressed.

The infrared spectrum of carbon dioxide on a sodium chloride film was first reported by Kozirovski and Folman [1]. They observed a single resonance in the asymmetric stretching region, and two bands in the bending region. Based on coverage behavior of the bending doublet Kozirovski and Folman concluded that there is one kind of adsorption site, and that carbon dioxide has a non-perpendicular orientation with respect to the surface. Also using a film, Heidberg and Singh have confirmed that the bending absorbance is split [10]. The heat of adsorption has been measured by Hayakawa as 26 kJ mol⁻¹ [11]. Theoretical calculations by Hayakawa [11], Heidberg et al. [12], and Depriek and Julg [13], while consistent with this value, are ambiguous concerning the nature of the preferred adsorption site.

Recently Heidberg and coworkers have published spectra of carbon dioxide on a single crystal substrate. They reported that the asymmetric stretch of ¹²C¹⁸O₂ at monolayer coverage gives a single absorbance band [7]. Subsequently they reported that the asymmetric stretch of ¹³C¹⁶O₂ at monolayer coverage yields a doublet [14]. We suspect that the discrepancy between these reports is due to surface contamination.

Our results for CO₂ on NaCl(100) are presented here. We have studied the system at a variety of coverages, temperatures, and polarization conditions. The observations are generally consistent with previous work. Our discussion of this system converges on a simple model: carbon dioxide is adsorbed in the form of two-dimensional, crystalline islands. We propose a structure for this phase and interpret details of the infrared spectrum in terms of its collective vibrational modes. The group-theoretical analysis that we apply makes use of the full symmetry group of a thin film, and is particularly useful for a physisorbed monolayer. We contrast our approach with other forms of symmetry analysis.

2. Equipment and procedures

Most of the experimental details are described elsewhere [8,9]; only an outline will be presented here. The substrate for adsorption was prepared from single-crystal boules of sodium chloride (Harshaw). These were cleaved along (100) planes to form 30 × 20 × 3 mm³ slabs whose large faces contacted nothing except air. The surfaces appeared clear and smooth, although some terracing was visible. Two slabs were mounted on a copper sample holder, which in turn was fixed to the work surface of an open-cycle liquid helium cryostat (Janis Research). A thermocouple and resistive heater within the work surface allowed temperature maintenance through an external controller (Lake Shore Cryotronics). Temperature accuracy at the NaCl(100) surface was checked by the onset of condensation of CO₂. The reported temperatures have

an accuracy of ± 1.0 K. The controller was able to maintain temperatures with a stability of ± 0.2 K.

The work surface of the cryostat and the sodium chloride crystals were sealed within an ultrahigh vacuum chamber, where an ion pump (Varian) maintained a base pressure of 9×10^{-10} mbar. The crystals were stored at 380 K between experiments. At this temperature all atmospheric molecules desorb, but the evaporation rate of sodium chloride itself is negligible [15]. This method of crystal preparation is known to produce extended, clean (100) faces with occasional steps of atomic dimensions [16]. Furthermore, we are now able to assess the cleanliness of the crystals by analyzing the vibrational spectrum of adsorbed carbon monoxide [9]. We are confident that the substrate for the experiments discussed below was sodium chloride (100).

Carbon dioxide ($^{12}\text{C}^{16}\text{O}_2$, Matheson, Research Grade) was used without additional purification. The gas was admitted to the vacuum chamber through a bleed valve and continuously pumped away; all pressure data represent steady states of a flow system. Pressures were measured with an ion gauge and corrected for the ionization cross section of CO_2 . Monolayer and submonolayer spectra were recorded only when the adsorbed phase was in equilibrium with the pressure in the chamber. Coverage, therefore, was strictly a function of temperature and pressure. The only temperature-controlled objects in the infrared beam were the sodium chloride crystals, and CO_2 gas density in the chamber was far too low for infrared detection.

The vacuum chamber was fitted with wedged calcium fluoride windows, and the NaCl crystals were mounted so as to allow transmission spectroscopy. A commercial Fourier transform infrared spectrophotometer (Mattson Nova Cygni 120) was used with a slight modification: the infrared beam emerging from the interferometer was carried to the remote sample and monitored by an external detector. The optical layout is described elsewhere [8,9]. The modulated, collimated beam was focused through the center of the vacuum chamber, then collected onto the element of a liquid nitrogen cooled indium antimonide detector. The beam passed through four crystal/vacuum interfaces, all of which were tilted 60° from its direction of propagation. The entire path of the infrared beam was purged with dry nitrogen gas; in this way, interference by atmospheric CO_2 was effectively eliminated.

A wire grid polarizer (Moletron) was placed in the infrared beam between the chamber and the detector. Although the radiation field at the sample was the same for all experiments, the polarizer selected a specific linearly polarized component for analysis: E_p -polarized in the plane of incidence, and E_s -polarized perpendicular to the plane of incidence.

Scanning and processing parameters were the same for all spectra. One hundred scans were coherently averaged, and the resulting interferogram was extended with zeros by a factor of four. No apodization function was employed. Before admitting gas to the sample chamber, separate background

spectra were recorded for every temperature/polarization condition under study. Sample spectra were ratioed against the appropriate backgrounds to produce absorbance plots. The integrated absorbance is defined as:

$$\tilde{A} = \int_{\text{band}} \log_{10}(I_0/I) d\tilde{\nu}, \quad (1)$$

where the appropriate subscript on \tilde{A} designates an E_s or E_p polarization measurement. Frequency accuracy and resolution were measured from absorbance features due to gas phase molecules. In the frequency range of interest, spectral resolution was 0.2 cm^{-1} (FWHM) and peaks appeared within $\pm 0.05 \text{ cm}^{-1}$ of their accepted positions. The observable frequency range, limited by the sample chamber windows and infrared detector, spanned from 1000 to 5000 cm^{-1} .

3. Results

When the crystals were cooled to less than 100 K and CO_2 gas was admitted to the sample chamber, infrared absorbances appeared in the asymmetric stretching region. The system was studied at three temperatures. Spectra are shown in figs. 1–3.

At 95.0 K no infrared signals are found for CO_2 pressures below 2.1×10^{-7} mbar. In the pressure range from 2.1×10^{-7} to 3.4×10^{-7} mbar, two well-resolved peaks are observed in both E_s and E_p polarizations. Fig. 1 shows that these signals are correlated with pressure. Below 3.4×10^{-7} mbar the absorbance scales reversibly with pressure, demonstrating that the coverage of CO_2 is at equilibrium. In the pressure range from 3.4×10^{-7} to 3.0×10^{-6} mbar no further increase in signal intensity is found. All spectra in fig. 1 were recorded at pressures below the vapor pressure of solid CO_2 , which is 3×10^{-6} mbar at 95 K [17]. Equilibrium between the adsorbed and gaseous phases was reached within 30 min of a change in pressure. Three qualities of these spectra are significant: first, the peak positions are independent of their intensity; second, the ratio of individual band areas is independent of their overall intensity (high-frequency/low-frequency = 0.2); finally, the integrated absorbance of the doublet saturates to a maximum value.

Two additional absorbance peaks are observed when the CO_2 pressure in the chamber is greater than the vapor pressure of CO_2 at the crystal temperature. When 6.9×10^{-8} mbar of CO_2 is exposed to crystals at 65.0 K , the two peaks found at 95.0 K are present at their saturation intensity. In addition, time-dependent signals appear at 2344 and 2382 cm^{-1} . Fig. 2 shows the behavior of these peaks at ten minute intervals, with temperature and pressure held constant. The position and intensity of the peaks observed in fig. 1 are independent of time. The new signals, however, grow indefinitely.

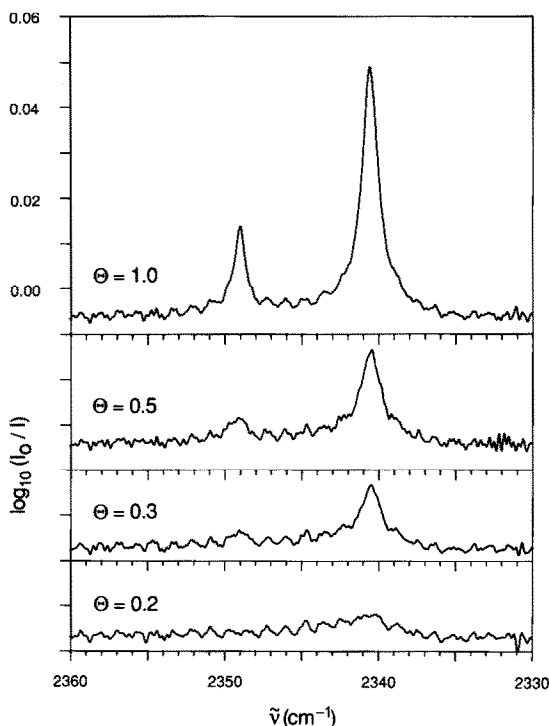


Fig. 1. CO₂ on NaCl(100) at 95.0 K. Equilibrium pressures ranged from 2.1×10^{-7} mbar ($\Theta = 0.2$) to 3.4×10^{-7} mbar ($\Theta = 1.0$). Spectra were recorded with E_p -polarized light.

At 86.2 K, under 3.4×10^{-8} mbar of CO₂ (not sufficient for condensation), the absorbance doublet saturates to the same band area as was observed at 95.0 K. Fig. 3 compares E_p and E_s spectra under these conditions. Combined band area is greater for E_s polarization ($\tilde{A}_s = 0.16 \text{ cm}^{-1}$) than for E_p polarization ($\tilde{A}_p = 0.13 \text{ cm}^{-1}$). This difference appears as absorbance intensity of the high-frequency resonance in the E_s experiment. The peak frequencies are 2349.0 and 2340.1 cm^{-1} , independent of polarization; the respective band widths (FWHM) are 0.4 and 0.7 cm^{-1} .

Our results in fig. 3 differ significantly from those of Heidberg and Hoge [7] for $^{12}\text{C}^{18}\text{O}_2$ on NaCl(100) at 75 K. They observed a single band with linewidth (FWHM) of 10 cm^{-1} , in contrast to our fully resolved doublet. Furthermore, the integrated absorbance of 0.007 cm^{-1} for their system at a claimed monolayer coverage is an order of magnitude smaller than either the E_p or E_s spectra in fig. 3. The simplest interpretation of the discrepancy is that the surfaces used by Heidberg and Hoge were badly damaged or contaminated. The more recent results of Heidberg et al. [14], using a mixture of isotopes, do indicate a doublet for $^{13}\text{C}^{16}\text{O}_2$ on NaCl(100). Once again the signals are weak

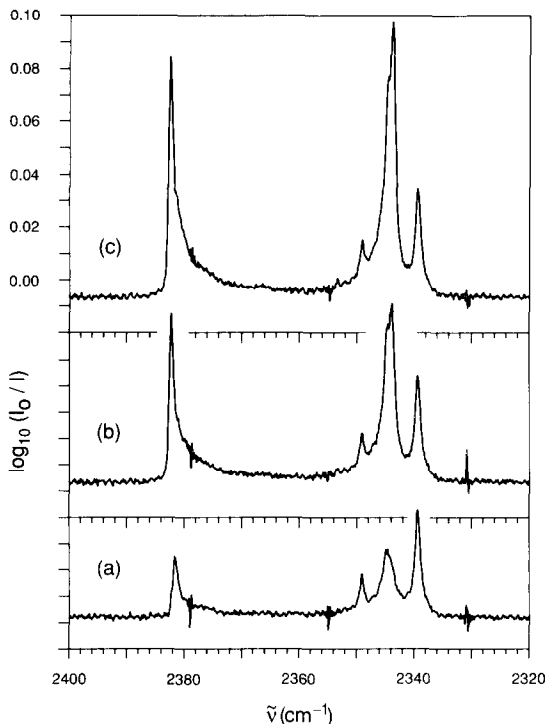


Fig. 2. Growth of CO₂ multilayers on NaCl(100) at 65.0 K. The CO₂ pressure, 6.9×10^{-8} mbar, was greater than its saturation pressure at this temperature. Spectra (a), (b) and (c) were recorded at ten minute intervals with E_p -polarized light.

and diffuse in comparison to those in fig. 3. It is not clear whether the isotopic dilution can account for the remaining discrepancies between our work and theirs.

4. Discussion

Our goal is to develop a structural model of the CO₂ monolayer on NaCl(100). We proceed through several steps. Qualitative arguments, based on the gross behavior of the system, are first used to eliminate several candidate explanations. Then polarization data are quantified to reveal angular information. Next, symmetry theory is applied to yield a monolayer structure. Finally, a theoretical model of intermolecular coupling is used to check the proposed structure.

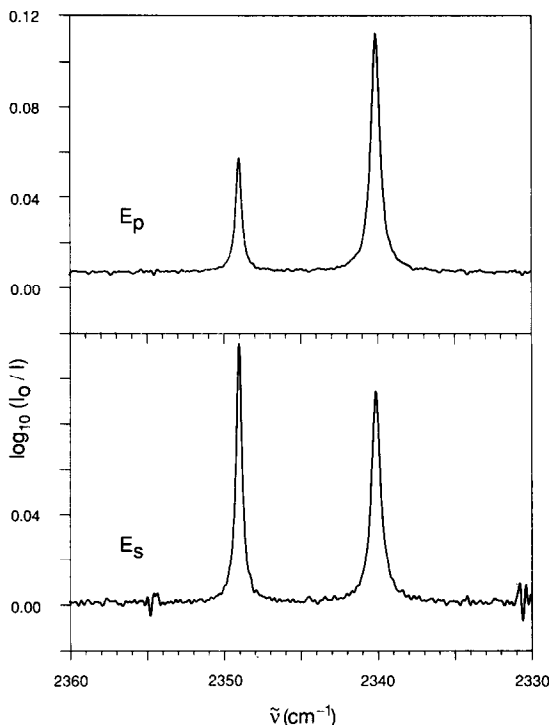


Fig. 3. Comparison of E_p and E_s polarization measurements of a CO_2 monolayer on $\text{NaCl}(100)$ at 86.2 K. Pressure was maintained at 6.9×10^{-8} mbar.

4.1. Correlation field splitting and island formation

The asymmetric stretching vibration of free CO_2 (ν_3) is nondegenerate. When adsorbed on sodium chloride, two infrared absorbances are found in this frequency region. Following are distinct mechanisms by which a nondegenerate internal vibration can be split during adsorption:

(A) Multiple trapping sites. If more than one kind of surface/adsorbate interaction is available, it is likely that these will perturb molecules in different ways. Thus a nondegenerate vibration will be shifted to a different degree by each kind of site. In the adsorbed phase, the population of each kind of site will give a distinct signal.

(B) Vibrational combination or sequence bands. Upon adsorption, the translational and rotational degrees of freedom of a gas phase molecule are converted to external vibrations (hindered translations and librations) of the surface/adsorbate bond. If these vibrations combine with the fundamental internal vibration then multiple features can be observed. Alternatively, a fundamental vibration can occur at slightly different frequencies as it originates from excited external levels. When these levels are populated, multiple resonances will result.

(C) Correlation field splitting. Consider a regular array of symmetry-related nondegenerate oscillators such that each is in the same local environment. If the oscillators are coupled, we must consider their motion collectively. One internal molecular vibration contributes n modes to the array, where n is the number of molecules per unit cell [18]. These modes may differ in energy, and consequently may produce multiple resonances. Factor group splitting is a different name for the same effect.

First, we examine whether mechanism A is plausible. In fig. 1 the peaks grow in tandem. This is inconsistent with the suggestion that two adsorption sites are responsible. Different sites are certain to have different heats of adsorption. Under equilibrium conditions this must lead to fractionation: at low coverage, the lower-energy (strongly adsorbing) sites are preferred. We would expect these sites and the corresponding absorbance peak to saturate at low coverage; the higher-energy sites and signal would fill in at higher coverage. This was not observed.

The same reasoning applies equally well if the second site is on top of molecules adsorbed directly to the crystal. Indeed, even if the fractional coverage of the bare surface and the fractional coverage of the first adsorbate layer (by a second layer) had the same pressure dependence, the *number* of molecules in each layer would not. Thus the ratio of corresponding band areas would not be constant.

Finally, fig. 2 shows that the absorbance due to *solid* CO₂ overlayers is distinct. The time-dependent signals appeared only when the substrate was below condensation temperature. The absorbance observed at 2344 cm⁻¹ matches the known resonance frequency of α -CO₂ [19]. Solid CO₂ is a cubic crystal; its active ν_3 vibration is triply degenerate. In the case of an extremely thin slab, however, the cubic symmetry is broken and the degeneracy of ν_3 is lifted. The resulting "longitudinal optical" mode is apparent at 2382 cm⁻¹ in fig. 2. We have observed and analyzed similar splitting in the spectra of CO multilayers [8]. For the present discussion it is sufficient to distinguish between monolayer and multilayer features.

We conclude that only one kind of adsorption site is involved. The saturated doublet is assigned to a monomolecular layer of CO₂ at a relative coverage of unity ($\Theta = 1$). The other coverage values given in fig. 1 are obtained from combined band areas and are normalized with respect to the saturation value.

Splitting mechanisms B are consistent with a one-site model. However, combination bands for physisorbed molecules are weak and diffuse [4]. Furthermore, a combination band consistent with our data (shifted by +9 cm⁻¹) would be accompanied by a low-frequency component (shifted by -9 cm⁻¹). No such feature was observed. Similarly, sequence structure would display multiple and temperature sensitive features. Only two monolayer signals are observed over the temperature range from 65 to 95 K (figs. 1-3).

This leaves mechanism C, correlation field splitting. In the case of a split molecular vibration, we can test for correlation effects by isotopic substitution. When a substituted oscillator is present in a crystal in low concentration, its static field is unchanged. However, its isotope-shifted vibrational frequency eliminates resonant coupling to the surrounding (unsubstituted) oscillators. Therefore, the low-concentration species cannot show correlation field splitting. There is preliminary evidence that this is the case for CO₂ on NaCl(100). We have performed experiments using highly divided sodium chloride films as substrates [20]. The high optical density of adsorbates on such films allows us to detect ¹³C¹⁶O₂ present in natural abundance (1%). Whereas the ¹²C¹⁶O₂ signal is a complex multiplet, the minority ¹³C¹⁶O₂ gives a single, sharp resonance. Similarly, Heidberg et al. have performed single-crystal experiments with a 8:1 (¹³C¹⁶O₂:¹³C¹⁶O¹⁹O) mixture [14]. Although ill-resolved, the ¹³C¹⁶O₂ band is split while the ¹³C¹⁶O¹⁸O peak is not. In addition to supporting mechanism C these observations are inconsistent with mechanisms A and B.

We conclude that the observed doublet is due to intermolecular coupling within an ordered layer of CO₂ molecules. Since two bands are observed, this layer has at least two molecules per unit cell. The resonances can be viewed as collective vibrations in a two-dimensional array of ν_3 oscillators.

With this in mind, we again consider the equilibrium submonolayer spectra of fig. 1. It is reasonable to assume that the degree of intermolecular vibrational coupling increases with increasing two-dimensional density of the CO₂ layer. If the molecules were forced into interaction by *crowding*, we expect that the onset and extent of correlation field splitting would depend on coverage. In fact, the splitting is as pronounced at $\Theta = 0.3$ coverage as at $\Theta = 1.0$. Since the splitting is not a function of coverage, neither is the density of the CO₂ layer in which it occurs. In other words, the layer grows in the form of fixed-density islands.

The preceding conclusion requires two qualifications. First, the spectra indicate island formation only if the observed splitting is a correlation field effect. If the doublet were due to mechanisms A or B, then even a randomly distributed submonolayer would have a split absorbance. Such a layer would be amorphous, however, and lack of translational symmetry excludes correlation effects. Therefore the observation of correlation field splitting at $\Theta = 0.3$ implies local crystalline order. Finally, it should be noted that our observation of submonolayer islands does not address the nature of diffusion along the surface. During these measurements the adsorbed phase was in dynamic equilibrium with the gas. Therefore all possible adsorption sites were continually sampled by thermal processes.

4.2. Photometric calculations

Our analysis now turns to the geometry of the adsorbed-CO₂ array. It was argued that all adsorption sites represented by the spectra are equivalent. The

site can be divided into two components: the relation of a CO₂ molecule to the sodium chloride surface, and the relation of a CO₂ molecule to neighbouring CO₂ molecules. Given an answer to the first problem, symmetry theory can be used to penetrate the second.

Information about adsorption geometry is found by comparing the absorbances of E_s and E_p polarized light. Consider, for example, a hypothetical adsorption geometry such that the bond axis is perpendicular to the surface. The molecular transition dipole for ν_3 has a component normal to the surface but none parallel. It can adsorb a component of E_p radiation, but is orthogonal to E_s . No E_s signal would be observed; clearly this is not the case for CO₂. On the other hand, the molecular transition dipole could be parallel to the surface. This would interact with E_s radiation and with the component of E_p parallel to the surface. Note that the active component of radiation in both polarizations is parallel to the surface and pointing in a [100] direction on the crystal. They differ only in absolute intensity (since the perpendicular component of E_p radiation is inert). The resulting absorbances, therefore, would differ only in absolute intensity. This is not the case for CO₂, either. The E_s and E_p spectra are qualitatively distinct. To account for this difference, the molecular transition dipoles (hence the collective transition dipoles which they

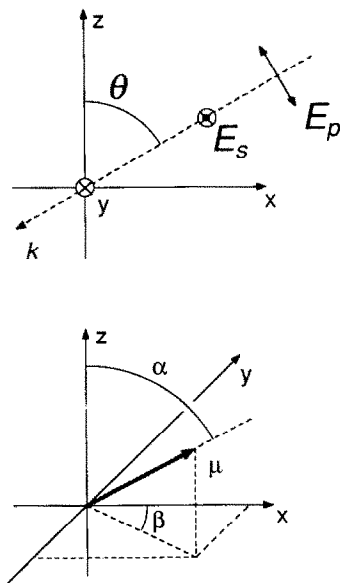


Fig. 4. Coordinate and angle definitions. The z axis is perpendicular to the NaCl(100) surface; the x and y axes point along [100] directions. The upper figure, an orthographic projection, shows the direction of propagation k and the electric field direction for E_p - and E_s -polarized light. The lower figure, a perspective projection, shows the orientation of a transition dipole μ .

form) must be sensitive to the perpendicular component of E_p radiation. In other words, the molecular axis must be oblique with respect to the surface.

Let us quantify this argument with relationships obtained directly from classical optics. We assume that the monolayer represents a thin film of oriented gas molecules on a homogeneous dielectric substrate. We say "oriented gas" because the adsorbed molecules are assumed to retain the electrical properties (e.g. integrated optical cross section, $\bar{\sigma}_g$) of isolated molecules.

The coordinate system is illustrated in fig. 4. The z -axis is chosen normal to the surface; the intersection of the plane of infrared incidence and the plane containing the surface is chosen as the x -axis. The y -axis, then, is in the plane of the surface and perpendicular to the plane of incidence. The upper portion of fig. 4 shows the vectors which describe the interrogating light at the surface. The angle of incidence of the propagation vector is $\theta = 60^\circ$ for our experiment. The lower portion of the figure defines the orientation of the molecular transition dipole, μ . The ν_3 transition dipole lies along the CO₂ molecular axis.

Expressions for integrated absorbance are obtained by resolving both the incident radiation and the integrated molecular cross section into x , y , and z components. For radiation incident on the substrate at Brewster's angle we have derived the following relations [9]:

$$\tilde{A}_p = \frac{NS}{2.303 \cos \theta} [\bar{\sigma}_z \sin^2 \theta + \bar{\sigma}_x \cos^2 \theta], \quad (2)$$

$$\tilde{A}_s = \frac{2NS}{2.303 \cos \theta (1 + n^2)} [\bar{\sigma}_y], \quad (3)$$

where N is the number of surfaces interrogated, S is the surface density of adsorbates, and $\bar{\sigma}_x$, $\bar{\sigma}_y$, $\bar{\sigma}_z$ are the components of integrated molecular cross section. The substrate is non-reflecting as well as non-absorbing for E_p radiation. E_s radiation, however, is partially reflected by the substrate. The effect of this reflection is to reduce \tilde{A}_s by a factor of $2/(1 + n^2)$, where n is the index of refraction of the substrate.

It remains to relate the integrated cross section of the gas phase molecule ($\bar{\sigma}_g$) to the effective integrated cross sections ($\bar{\sigma}_x$, $\bar{\sigma}_y$, $\bar{\sigma}_z$) of an oriented molecule. The empirical $\bar{\sigma}_g$ is an average over all orientations and the components of the transition dipole μ are shared equally among the three Cartesian coordinates. If a molecule is locked *parallel* to the probing electric field, its integrated cross section becomes $3\bar{\sigma}_g$. For a general orientation this is reduced by a function of angles α and β . Projections of the transition dipole along the space-fixed x , y , and z axes couple with the corresponding components of the electric field E . The projection is accomplished with direction cosines [21].

Evaluation of $|\boldsymbol{\mu} \cdot \mathbf{E}|^2$ produces the trigonometric terms in the equations below:

$$\bar{\sigma}_x = 3\bar{\sigma}_g \sin^2\alpha \cos^2\beta, \quad (4)$$

$$\bar{\sigma}_y = 3\bar{\sigma}_g \sin^2\alpha \sin^2\beta, \quad (5)$$

$$\bar{\sigma}_z = 3\bar{\sigma}_g \cos^2\alpha. \quad (6)$$

Subscripts x , y , z specify the field direction to which each component is sensitive. Should molecules become locked along the z -direction, as is the case for CO on NaCl(100) [9], then $\alpha = 0^\circ$ and $\bar{\sigma}_z = 3\bar{\sigma}_g$, and $\bar{\sigma}_x = \bar{\sigma}_y = 0$. For CO₂, we will find that all components of integrated cross section are non-zero.

The angle β requires special consideration. There are four equivalent directions on the NaCl(100) surface, but this may not be true of the CO₂ layer. It is possible that the adsorbate forms separate, structurally equivalent rotational domains distinguished only by the value of β . Our experiment probes macroscopic regions of four surfaces; we can be certain that a large number of independently nucleated islands are present. Therefore, the spectra represent the average behavior over all possible rotational domains. To incorporate this in the photometric model, we average eqs. (4) and (5) over an even distribution of β . Using $\langle \sin^2\beta \rangle = \langle \cos^2\beta \rangle = 1/2$ we obtain:

$$\bar{\sigma}_x = \frac{3}{2}\bar{\sigma}_g \sin^2\alpha, \quad (7)$$

$$\bar{\sigma}_y = \frac{3}{2}\bar{\sigma}_g \sin^2\alpha. \quad (8)$$

On substitution of eqs. (6)–(8) into eqs. (2) and (3) the ratio of integrated absorbances becomes

$$\frac{\tilde{A}_p}{\tilde{A}_s} = (1 + n^2) \left[\frac{\cos^2\alpha + \sin^2\theta + (1/2) \sin^2\alpha \cos^2\theta}{\sin^2\alpha} \right]. \quad (9)$$

Solving for α , with $\theta = 60^\circ$,

$$\alpha = \tan^{-1} \left\{ \frac{6}{\left[8(\tilde{A}_p/\tilde{A}_s)/(1 + n^2) \right] - 1} \right\}^{1/2}. \quad (10)$$

To calculate α , the molecular tilt angle, with eq. (10) we use the ratio of total integrated absorbances $\tilde{A}_p/\tilde{A}_s = 0.81$. For sodium chloride the index of refraction is $n = 1.52$ [22]. Eq. (10) gives $\alpha = 68^\circ$.

With molecular tilt determined, eqs. (2) and (3) can be used individually to predict integrated absorbances. We use $N = 4$, $\theta = 60^\circ$, $\bar{\sigma}_g = 1.1 \times 10^{-16}$ cm molecule⁻¹ [23]. The adsorbate density is chosen to be the same as the density of sodium-chlorine ion pairs at the surface, $S = 6.3 \times 10^{14}$ cm⁻². This will be justified below. For the E_p experiment, the predicted value of \tilde{A}_p is 0.15 cm⁻¹,

while 0.13 cm^{-1} was observed. For E_s the predicted area is $\tilde{A}_s = 0.18 \text{ cm}^{-1}$, while 0.16 cm^{-1} was observed. Considering the $\sim 10\%$ error typical in measurements of gas phase integrated cross section [23,24], the agreement in the observed and predicted \tilde{A} values is good.

Eq. (10) has been derived for the total integrated absorbance of each polarization. We can use it with another interpretation based on our conclusion that the observed doublet is a consequence of correlation field splitting. Each resonance is a distinct collective (e.g. in-phase or out-of-phase) ν_3 vibration of the CO_2 layer. The transition dipole of such a lattice mode need not be parallel to any of the molecular transition dipoles from which it is composed. The band area ratio (\tilde{A}_p/\tilde{A}_s) for the high frequency signal is 0.45, which suggests a tilt angle for this transition dipole of $\alpha = 84^\circ$. The ratio is 1.1 for the low frequency resonance, which corresponds to a transition dipole tilt of $\alpha = 62^\circ$. These angles will be used later to assign the symmetry of the doublet components.

Considering its simplicity, the oriented gas model is in remarkable agreement with the data. There are several neglected physical mechanisms which lead us to expect greater discrepancy. First, all perturbations of the ν_3 vibrational mode have been ignored. It is not the case that the infrared cross section is conserved during a condensation. For example, CO_2 molecules have a 25% smaller cross section in their solid phase than as a gas [24]. Second, the optical behavior of the surface/adsorbate system has been oversimplified. The CO_2 layer is dense enough to have a significant index of refraction. Furthermore, induction effects in the substrate and CO_2 layer alter the transmittance properties of the sample. These complications have been explored in detail for a similar system, CO on $\text{NaCl}(100)$ [9,25]. In the present case it appears that the effects are relatively small or offset one another.

The transition dipole tilt angle α (for molecule or collective modes) was calculated from a *ratio* of angular dependences. Since the limiting magnitude of the integrated infrared cross section is represented equally in E_s and E_p band areas, it drops out of the expression for α . Furthermore, induced dipoles are expected to play comparable roles in altering \tilde{A}_s and \tilde{A}_p integrated absorbances. The value of α is therefore relatively insensitive to these effects.

4.3. Plane group symmetry analysis

The system of *one* carbon dioxide molecule adsorbed on $\text{NaCl}(100)$ has been examined through theoretical calculations [11–13]. Heidberg et al. identify three minima in the adsorption potential: (i) CO_2 molecule perpendicular to the surface over a sodium ion site; (ii) CO_2 molecule parallel to the surface, bridging two nearest-neighbor sodium ion sites; (iii) carbon atom of CO_2 equidistant from neighboring sodium and chlorine nuclei, molecule tilted by 45° toward chlorine atom (fig. 5).

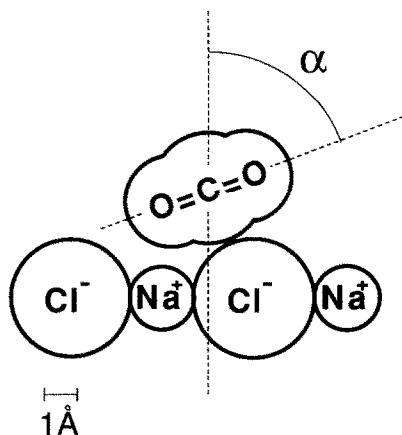


Fig. 5. Proposed oblique adsorption geometry. Outlines indicate the van der Waals contour of CO₂ and the ionic radii of Na⁺ and Cl⁻. All pictured nuclei are coplanar. The location of the carbon atom is as calculated by Heidberg et al. for this site [12]. Tilt angle $\alpha = 68^\circ$ was determined from the spectra in fig. 3.

Due to the sensitivity of calculated heats of adsorption to certain parameters, Heidberg et al. do not claim that this calculation can resolve the preferred site. Our results, however, are only consistent with the oblique geometry. In this discussion it is assumed that molecules are adsorbed at the oblique sites (as fig. 5), with the observed tilt angle $\alpha = 68^\circ$. It remains to construct a lattice of such adsorbates which is consistent with the spectra when correlation field coupling is invoked.

Our discussion of intermolecular geometry begins with two sound assumptions. First, it is assumed that the island-phase CO₂ molecules are packed at a density of one per exposed sodium-chlorine pair, or $6.3 \times 10^{14} \text{ cm}^{-2}$ (one molecule per *surface* unit cell). This is 6% lower than the density in a two-dimensional (100) slice of α -solid CO₂ [26]. The intermolecular forces which dominate condensation (quadrupole-quadrupole) [27] and vibrational frequency shifts (dipole-dipole) [28] in the bulk solid are likely to be responsible for similar effects in a physisorbed phase. A regular, registered layer of lower density would separate the molecules considerably, and new coupling mechanisms would be required. A regular, registered layer of higher density is sterically impossible. In any case, absolute density does not affect the results of symmetry analysis.

Second, the absorbed infrared wavelengths are four orders of magnitude larger than the dimensions of a CO₂ molecule. We are therefore justified in the approximation that the radiation field is spatially invariant. A spatially invariant field can only excite vibrations which have a wave vector equal to zero. This can be stated as a selection rule: In order to be infrared active, a

collective vibrational mode must be totally symmetric with respect to translation. In other words, all unit cells must vibrate in phase [18,29,30].

The application of symmetry theory to a monomolecular layer is analogous to the treatment of other molecular crystals: the activity, degeneracy, and number of vibrational modes in an ordered phase can be predicted if its structure is known. In the present case, symmetry analysis is used to check whether proposed structural models are consistent with the observed spectroscopic activity.

Based on our observations, we have argued that every adsorbed CO₂ molecule is in an identical environment, therefore that intermolecular coupling is responsible for the ν_3 doublet. Accordingly, the structural information which can be extracted from the splitting concerns *intermolecular* geometry. In the following discussion the NaCl surface serves only as a template – it sets the inter-adsorbate distances and directions of tilt for any proposed structure. For symmetry analysis and intermolecular coupling calculations the adsorbed layer is considered in isolation. In effect, the layer is modeled as a crystal of CO₂ molecules which are restricted to a two-dimensional lattice.

If a structure is periodic in three dimensions, its symmetry is described by one of 230 space groups [31]. Because an ordered monolayer has only two degrees of translational symmetry its analysis is restricted to 80 plane groups [32]. These describe the 80 unique patterns which can be produced by repeating a three-dimensional unit cell on the points of a two-dimensional lattice. Plane groups include nonsymmorphic elements: screw axes (C^s) and glide planes (σ^g). This treatment is appropriate for the general case of a monomolecular layer since all nuclei are not necessarily coplanar. The plane groups are to be distinguished from the 17 two-dimensional space groups of crystallography, which are strictly planar [31]. Descriptions of the plane groups are not widely available. Therefore they are enumerated in table 1, adapted from Bhagavantam and Venkatarayudu [32].

The coordinate system which was used in the previous section (x, y, z) is not necessarily the natural system for symmetry analysis. Therefore we introduce Cartesian coordinates a, b , and c . Axes a and b are parallel to the plane of translational symmetry, the c -axis is perpendicular to it. Clearly the c and z axes are parallel, and the ab plane is parallel to the xy plane. Symmetry operations and point groups are denoted by Schoenflies notation. Specifically, C_a indicates 180° rotation about an axis parallel to a ; σ_a indicates reflection by a plane normal to a . C_a^s and σ_a^g are analogous, but include fractional translation. All C_3, C_4 , and C_6 axes are normal to the plane of translational symmetry (parallel to c). Other symbols in table 1 are used in accordance with their standard interpretations [21].

Pure translational operations exist for all of the plane groups, but they are not listed in table 1. When the common set of translations is factored out of the plane groups, the resulting “factor groups” are isomorphic to point groups

Table 1
Plane groups and factor groups

Bravais lattice	Plane group		Bravais lattice	Plane group		Factor group
	No	Operations		No	Operations	
Oblique	1	E	Centered rectangular	40	E C _a	C ₂
	2	E C _c		41	E σ _a	C _s
	3	E i		42	E C _c σ _a σ _b	C _{2v}
	4	E σ _c		43	E C _a C _b C _c	D ₂
	5	E C _c i σ _c		44	E C _a σ _b σ _c	C _{2v}
	6	E σ _a ²		45	E C _a i σ _a	C _{2h}
	7	E C _c i σ _c ²		46	E C _a C _b C _c i σ _a σ _b σ _c	D _{2h}
Primitive rectangular	8	E C _a	Square	47	E C _a ^s σ _b σ _c ²	C _{2v}
	9	E σ _a		48	E C _a C _b C _c i σ _a σ _b σ _c ²	D _{2h}
	10	E C _c σ _a σ _b		49	E C ₄ C ₄ C ₂	C ₄
	11	E C _a C _b C _c		50	E S ₄ S ₄ C ₂	S ₄
	12	E C _a i σ _a		51	E C ₄ C ₄ C ₂ i S ₄ S ₄ σ _h	C _{4h}
	13	E C _a σ _b σ _c		52	E 2C ₄ C ₂ 2σ _v ² 2σ _v ²	C _{4v}
	14	E C _a C _b C _c i σ _a σ _b σ _c		53	E C ₂ 2C ₂ ² 2S ₄ 2σ _v	D _{2d}
	15	E C _a ^s		54	E C ₂ 2C ₂ ² 2S ₄ 2σ _v ²	D _{2d}
	16	E σ _a ²		55	E 2C ₄ C ₂ 2C ₂ ² 2C ₂ ²	D ₄
	17	E C _c σ _a ² σ _b		56	E 2C ₄ C ₂ 2C ₂ ² 2C ₂ ² i 2S ₄ σ _h 2σ _v ² 2σ _v ²	D _{4h}
18	E C _c σ _a ² σ _b ²	57	E C ₄ C ₄ C ₂ i S ₄ S ₄ σ _h	C _{4h}		
19	E C _a ^s C _b C _c	58	E 2C ₄ C ₂ 2σ _v ² 2σ _v ²	C _{4v}		
20	E C _a ^s C _b ^s C _c					

21	$E_C^s i \sigma_a$	C _{2h}	59	$E 2C_4 C_2 2C_2'^s 2C_2''$	D ₄
22	$E_C^s i \sigma_b^g$		60	$E C_2 2C_2'^s 2S_4 2\sigma_v'$	D _{2d}
23	$E_C^s i \sigma_a^g$		61	$E C_2 2C_2'' 2S_4 2\sigma_v''^s$	D _{2d}
24	$E_C^s \sigma_b^g \sigma_c$	C _{2v}	62	$E 2C_4 C_2 2C_2'^s 2C_2''$	D _{4h}
25	$E_C^s \sigma_b \sigma_c^g$		$i 2S_4 \sigma_h 2\sigma_v''^s 2\sigma_v''$		
26	$E_C^s \sigma_b^g \sigma_c^g$		$E 2C_4 C_2 2C_2' 2C_2''$		
27	$E_C^s \sigma_b^g \sigma_c$		$i 2S_4 \sigma_h^g 2\sigma_v''^s 2\sigma_v''$		
28	$E_C^s \sigma_b^g \sigma_c^g$		$E 2C_4 C_2 2C_2'^s 2C_2''$		
29	$E_C^s \sigma_b \sigma_c^g$		$i 2S_4 \sigma_h^g 2\sigma_v'' 2\sigma_v'$		
30	$E_C^s \sigma_b \sigma_c$	Hexagonal	65	$E C_3 C_3$	C ₃
31	$E_C^s C_b C_c i \sigma_a^g \sigma_b \sigma_c^g$		66	$E C_3 C_3 i S_6 S_6$	S ₆
32	$E_C^s C_b C_c i \sigma_a^g \sigma_b^g \sigma_c^g$		67	$E 2C_3 3\sigma_v$	C _{3v}
33	$E_C^s C_b C_c i \sigma_a \sigma_b^g \sigma_c$		68	$E 2C_3 3C_2$	D ₃
34	$E_C^s C_b C_c i \sigma_a \sigma_b \sigma_c^g$		69	$E 2C_3 3C_2 i 2S_6 3\sigma_v$	D _{3d}
35	$E_C^s C_b C_c i \sigma_a^g \sigma_b^g \sigma_c^g$		70	$E C_3 C_3 \sigma_h S_3 S_3$	C _{3h}
36	$E_C^s C_b C_c i \sigma_a \sigma_b \sigma_c$		71	$E C_6 C_6 C_3 C_3 C_2$	C ₆
37	$E_C^s C_b C_c i \sigma_a^g \sigma_b^g \sigma_c$		72	$E C_6 C_6 C_3 C_3 C_2$	C _{6h}
38	$E_C^s C_b C_c i \sigma_a \sigma_b^g \sigma_c^g$		$i S_6 S_6 S_3 S_3 \sigma_h$		
39	$E_C^s C_b C_c i \sigma_a \sigma_b \sigma_c^g$		73	$E 2C_3 3C_2 \sigma_h 2S_3 3\sigma_v$	D _{3h}
			74	$E 2C_6 2C_3 C_2 2C_2' 3C_2''$	D ₆
			75	$E 2C_6 2C_3 C_2 3\sigma_v 3\sigma_v'$	C _{6v}
		76	$E 2C_3 3C_2'$	D ₃	
		77	$E 2C_3 3\sigma_v'$	C _{3v}	
		78	$E 2C_3 3C_2' i 2S_6 3\sigma_v'$	D _{3d}	
		79	$E 2C_3 3C_2' \sigma_h 2S_3 3\sigma_v'$	D _{3h}	
		80	$E 2C_6 2C_3 C_2 3C_2' 3C_2''$	D _{6h}	
		$i 2S_6 2S_3 \sigma_h 3\sigma_v' 3\sigma_v''$			

[18,29]. This reduction obtains when nonsymmorphic operations (C^s and σ^s) are interpreted as simple rotation and reflection. Appropriate factor groups are listed in table 1.

The discussion in preceding sections can be used to identify constraints on the symmetry of the CO₂ layer. First, consider the possibility of rotational axes perpendicular to the layer. Since the molecules are tilted, their collective in-phase ν_3 vibration must be infrared active. If any C_c exists, the transition dipole for this mode must also be perpendicular to the layer. However, both active modes were observed in the E_s -polarized experiment. Each must have a component of its transition dipole parallel to the layer. Therefore the layer has no C_c (or C_3 , C_4 , C_6) axes. This eliminates 54 of the 80 plane groups from consideration.

Second, we apply the assumption that the wave vector is exactly zero for the observed vibrations. The active modes are totally symmetric with respect to translation. This allows pure translational operations to be factored out of the plane groups, leaving the factor groups which we have identified in table 1. Therefore active vibrational modes are described by the character table of an isomorphic point group. Notice that the "principal" rotational axis of a factor group can be either parallel or perpendicular to the plane of translational symmetry. The coordinates of published character tables must be carefully transformed into the a , b , c system. For example, plane group #23 has factor group C_{2h} . Table 2 is the corresponding character table in a , b , c coordinates. This table will be used presently.

The 26 remaining plane groups represent six factor groups: C_1 , C_2 , C_i , C_s , C_{2h} , and C_{2v} . Further eliminations are made by considering the character tables appropriate for these groups. The observed unit cell contains at least two symmetry-related molecules, which produce two nondegenerate infrared active vibrational modes. Factor groups C_1 and C_i are insufficient. Also, one of the observed transition dipoles is oblique with respect to the layer; it interacts with at least two components of the electric field vector (including E_z). Therefore factor group C_{2v} is impossible. We are left with 14 plane groups, which reduce to factor groups C_2 , C_s , C_{2h} .

Finally, prospective structures are considered. There is no upper limit to the number of molecules per unit cell. In order to find the simplest model which is

Table 2
Character table: C_{2h} isomorphic plane group

	E	C_2^s	i	σ_h^s
A_g	1	1	1	1
B_g	1	-1	1	-1
A_u	1	1	-1	-1 (μ_a)
B_u	1	-1	-1	1 (μ_b, μ_c)

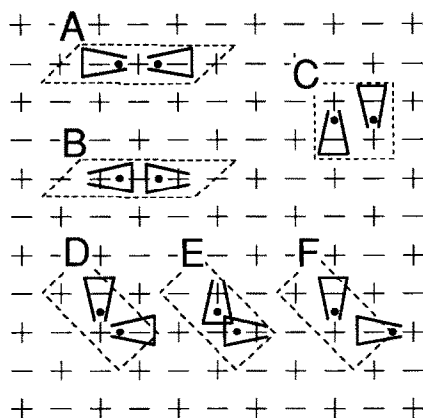


Fig. 6. Schematic of six possible CO₂ arrays. Each has two molecules per primitive unit cell of the layer, and each has an overall density of one molecule per surface unit cell. A triangle represents one CO₂ molecule tilted out of the plane of the illustration (in a fig. 5 type site); heavy dots represent carbon atoms; (+) and (-) represent underlying ions. Broken lines indicate the boundaries of a layer unit cell.

consistent with our data, we first evaluate structures with the lowest possible number: two. Having assumed an adsorbate density of one molecule per *surface* unit cell, and using the adsorption site from fig. 5, six different structures are possible. Unit cells for these six layers are illustrated in fig. 6. Arrays A, B, and C have C_c axes. They do not fall among the allowed plane groups, therefore we eliminate them. The layers defined by unit cells D and E have factor group C_s , but pairs of CO₂ molecules share single sodium or chlorine ions. Because of this unlikely steric crowding (see fig. 5) we rule out cells D and E in favor of F.

An extended portion of the proposed geometry is illustrated in fig. 7. The layer exhibits four symmetry operations: identity (E), inversion (i), screw rotation (C_a^s), and glide reflection (σ_a^g). These form a primitive rectangular plane group (#23) which is analogous to the C_{2h} point group. The appropriate character table (in coordinate system a, b, c) is given as table 2. The unit cell contains two molecules, therefore it has two collective ν_3 modes. The out-of-phase combination is in symmetry representation A_u . It is infrared active, with a transition dipole parallel to the a -axis (parallel to the layer). The in-phase combination is in symmetry class B_u . It is infrared active with an oblique transition dipole in the bc plane. On geometric grounds the collective in-phase dipole is expected to be tilted 60° from the layer normal. We may now use the results from the photometry section to assign the symmetry representations to the observed resonances. The high frequency vibration, 2349.0 cm^{-1} , was determined to have its transition dipole tilted to $\alpha = 84^\circ$. We now associate this resonance with the A_u -symmetric mode ($\alpha = 90^\circ$). The

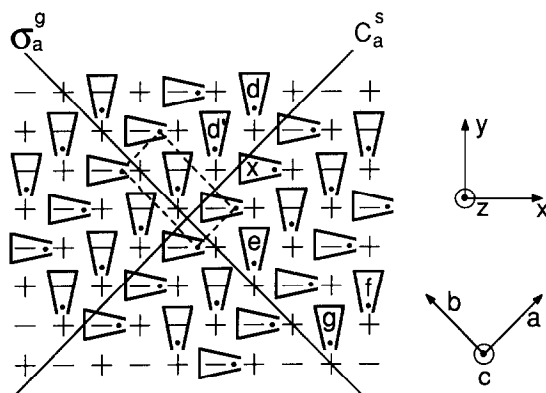


Fig. 7. Proposed structure of the CO_2 layer. A primitive unit cell (F from fig. 6) is outlined. The x , y , z coordinates of fig. 5 are shown. Coordinate system a , b , c is used for symmetry analysis (tables 1 and 2). In addition to glide planes and screw axes, the layer exhibits a center of inversion at each carbon atom. The five closest pairs of nonequivalent molecules are indicated as d , d' , e , f , and g in combination with molecule x .

low frequency component, 2340.1 cm^{-1} , is associated with B_u mode. The tilt of this transition dipole, found to be $\alpha = 62^\circ$, is close to the geometric value of 60° .

The structure proposed in fig. 7 is the only two-molecule array which is thoroughly consistent with our observations. The unit cell has four distinct orientations. Therefore four rotational domains are indeed possible. It is interesting that the proposed structure is a slightly distorted analogue of the densest sheet of molecules found in solid $\alpha\text{-CO}_2$ [26].

Our data provide one detail about the molecular adsorption site: the tilt angle α . Because of inter-adsorbate forces, it is likely that the true adsorption site is a modification of the one shown in fig. 5. The precise molecule-to-surface geometry is still unknown. In the preceding discussion, accordingly, the symmetry-breaking properties of the substrate were suppressed. We have used plane group analysis because of its coherence with an oriented gas model of physisorption; its level of articulation matches the unique and limited nature of our spectra. We observe correlation field splitting of one nondegenerate, internal molecular vibration. The symmetry restrictions developed above are the most that the ν_3 mode can reveal.

When the substrate is included in the symmetry analysis, the complete unit cell can not exhibit inversion centers or in-plane rotational axes. It is restricted to two-dimensional space group symmetry [31]. The study of adsorbate vibrations from this perspective has been reviewed by Richardson and Shepard [30]. Under these restrictions the proposed $\text{NaCl}(100)/\text{CO}_2$ structure has two symmetry operations: identity and glide reflection. The corresponding

factor group is C_2 . The activity of ν_3 vibrations of the unit cell, as described by the C_2 character table, is consistent with our spectra.

4.4. Dipolar coupling calculations

The proposed structure is in quantitative agreement with our data. We can test the model further by considering the magnitude of its correlation field splitting. In many molecular crystals the dominant contribution to this effect is from transition dipole–transition dipole interaction. To model these dipolar interactions is a natural first step. In the present case, the transition dipole μ connects the $v = 1$ and $v = 0$ states of the ν_3 vibration in CO_2 . Given a lattice geometry, we can use theory to predict the extent of collective mode splitting as a function of the transition dipole.

The transition dipole is simply related to the integrated molecular cross section:

$$\bar{\sigma}_g = (8\pi^3 \bar{\nu} / 3ch) |\mu|^2, \quad (11)$$

where, following Yardley [33], we will use cgs units. The frequency of the vibration is given by $\bar{\nu}$; c and h are the speed of light and Planck's constant, respectively. Using the gas phase result $\bar{\sigma}_g = 1.1 \times 10^{-16}$ cm molecule⁻¹ [23] and $\bar{\nu} = 2345$ cm⁻¹ (an average of the doublet transition frequencies) we arrive at $|\mu| = 3.4 \times 10^{-19}$ gm^{1/2} cm^{5/2} s⁻¹, or 0.34 debye.

Hexter has developed a vibrational exciton model for vibrational coupling in crystals [34]. The theory considers perturbations due to pairwise transition dipole interaction. He simplifies the problem by counting such interaction only within a two-dimensional sheet of molecules. The geometry considered by Hexter is isomorphic to the CO_2 array proposed in fig. 7. He develops an analytical expression relating the molecular transition dipole to the extent of correlation field splitting that it causes, $\Delta\bar{\nu}$. The formula (adapted from ref. [34], eqs. (35)–(38)) is directly applicable to the present case:

$$\Delta\bar{\nu} = (|\mu|^2/hc)[4(d + d' + e + f) + 2g], \quad (12)$$

where d , d' , e , f , g are geometric terms which describe the five nearest nonequivalent dipole–dipole pairs. All the geometric terms have the following form:

$$d = (1/R_{d,x}^3)[2 \cos B_d \cos B_x - \sin B_d \sin B_x \cos \xi_{d,x}], \quad (13)$$

where dipoles “d” and “x” form the pair. The angle between one dipole and the line connecting the pair is B . The distance between the pair is R . Each dipole defines a plane with the connecting line; ξ is the angle between these planes. The five relevant types of pairs (d , d' , e , f , g) are shown in fig. 7 with respect to a central molecule (x). With the value of $|\mu|$ just given, the

NaCl lattice constant (5.64 Å [35]), and the array geometry of fig. 7, eq. (12) predicts a 20 cm^{-1} splitting; 9 cm^{-1} was observed.

The vibrational exciton model is quite sensitive to the spatial arrangement, of the dipole array. Its rough agreement with the measured splitting energy indicates that the proposed structure is self-consistent, and that correlation field splitting provides a satisfactory explanation of the observed doublet. The agreement between theory and experiment will improve when induction effects, higher-order couplings, and thermal shifts are included in the model [36–39]. In particular, calculations by Chen and Schaich [38] demonstrate the importance of electronic polarizability in attenuating the dipolar coupling among adsorbed CO₂ molecules.

5. Conclusions

Carbon dioxide can be physisorbed on the (100) face of sodium chloride crystals. Structural properties of the layer can be deduced from its infrared spectrum. We have observed the molecular asymmetric stretch and have developed a coherent account of its behavior upon adsorption. Following are the principal conclusions:

- (i) There is one preferred adsorption site;
 - (ii) in this site, the molecular axis of the adsorbate is oblique with respect to the surface;
 - (iii) the adsorbate layer grows in the form of constant-density islands;
 - (iv) a vibration–vibration coupling mechanism is active within these islands.
- It is therefore natural to interpret the vibrational behavior as that of a two-dimensional molecular crystal. The adsorbed layer is analogous to other systems consisting of sheets of molecules, such as Langmuir–Blodgett films and polymeric membranes. Plane group symmetry analysis is required for the full description of such systems.

It is clear that infrared spectroscopy can yield diverse and detailed information about a physisorbed phase. Some of our conclusions are well suited to verification by alternate experimental methods, such a electron and helium beam diffraction. Furthermore, there are potentially interesting thermodynamic and optical properties of CO₂ on NaCl(100) which have not been properly explored.

Acknowledgments

We have benefited from discussions with W.L. Schaich and W. Chen. The financial support of the National Science Foundation is acknowledged.

References

- [1] Y. Kozirovski and M. Folman, *Trans. Faraday Soc.* 62 (1966) 1431.
- [2] R.St.C. Smart, *Trans. Faraday Soc.* 67 (1971) 1183.
- [3] A. Zecchina and D. Sacrano, *Surface Sci.* 166 (1985) 347.
- [4] H.H. Richardson, C. Baumann and G.E. Ewing, *Surface Sci.* 185 (1987) 15.
- [5] J. Heidberg, H. Stein and I. Hussla, *Surface Sci.* 162 (1985) 470.
- [6] H.H. Richardson and G.E. Ewing, *J. Phys. Chem.* 91 (1987) 5833.
- [7] J. Heidberg and D. Hoge, *Surface Sci.* 189/190 (1987) 448.
- [8] H.-C. Chang, H.H. Richardson and G.E. Ewing, *J. Chem. Phys.* 89 (1988) 7561.
- [9] H.H. Richardson, H.-C. Chang, C. Noda and G.E. Ewing, *Surface Sci.* 216 (1989) 93.
- [10] J. Heidberg, R.D. Singh and H. Stein, *Ber. Bunsenges. Phys. Chem.* 82 (1978) 54.
- [11] T. Hayakawa, *Bull. Chem. Soc. Japan* 30 (1957) 124, 236, 243, 332.
- [12] J. Heidberg, R.D. Singh and C.F. Chen, *Z. Phys. Chem. (NF)* 110 (1978) 135.
- [13] B. Deprick and A. Julg, *Chem. Phys. Letters* 110 (1984) 150.
- [14] J. Heidberg, D. Hoge, K. Stahmer, H. Stein, M. Venschott, M. Warskulat and H. Weiss, *Vacuum* 38 (1988) 275.
- [15] J.E. Lester and G.A. Somorjai, *J. Chem. Phys.* 49 (1968) 2940.
- [16] G.A. Bassett, *Phil. Mag.* 3 (1958) 1042.
- [17] C.H. Meyers and M.S. Van Dusen, *J. Res. Natl. Bur. Std.* 10 (1933) 381.
- [18] P.M.A. Sherwood, *Vibrational Spectroscopy of Solids* (Cambridge Univ. Press, London, 1972).
- [19] W.E. Osberg and D.F. Hornig, *J. Chem. Phys.* 20 (1952) 1345.
- [20] O. Berg, unpublished results.
- [21] E.B. Wilson, Jr., J.C. Decius and P.C. Cross, *Molecular Vibrations* (McGraw-Hill, New York, 1955).
- [22] E.D. Palik, Ed., *Handbook of Optical Constants of Solids* (Academic Press, Orlando, FL, 1985).
- [23] S.S. Penner, *Quantitative Molecular Spectroscopy and Gas Emissivities* (Addison-Wesley, Reading, MA, 1959).
- [24] H. Yamada and W.B. Person, *J. Chem. Phys.* 41 (1964) 2478.
- [25] W.L. Schaich and W. Chen, *Phys. Rev.*, in press.
- [26] R.W.G. Wyckoff, *Crystal Structures*, Vol. 1, 2nd ed. (Interscience, New York, 1963).
- [27] A.D. Buckingham, *Quart. Rev.* 13 (1959) 87.
- [28] D.A. Dows and V. Schettino, *J. Chem. Phys.* 58 (1973) 5009.
- [29] R. Zbinden, *Infrared Spectroscopy of High Polymers* (Academic Press, New York, 1964).
- [30] N.V. Richardson and N. Sheppard, *Normal Modes at Surfaces*, in: *Vibrational Spectroscopy of Molecules on Surface*, Eds. J.T. Yates and T.E. Madey (Plenum, New York, 1987).
- [31] N.F.M. Henry and K. Lonsdale, Eds., *International Tables for X-ray Crystallography*, Vol. 1 (Kynoch, Birmingham, England, 1952).
- [32] S. Bhagavantam and T. Venkatarayudu, *Theory of Groups and Its Application to Physical Problems* (Academic Press, New York, 1969).
- [33] J.T. Yardley, *Introduction to Molecular Energy Transfer* (Academic Press, New York, 1980).
- [34] R.M. Heister, *J. Chem. Phys.* 33 (1960) 1833.
- [35] G. Benedek, G. Brusdeylus, R.B. Doak, J.G. Skofronick and J.P. Toennies, *Phys. Rev. B* 28 (1983) 2104.
- [36] G.D. Mahan and A.A. Lucas, *J. Chem. Phys.* 68 (1978) 1344.
- [37] B.N.J. Persson and R. Ryberg, *Phys. Rev. B* 24 (1981) 6954.
- [38] W. Chen and W.P. Schaich, *Surface Sci.* 220 (1989) L733.
- [39] C. Noda, H.H. Richardson and G.E. Ewing, to be published.